The Open Neuroimaging Journal
DOI: 10.2174/0118744400493253260715094516, 2026, 19, e18744400493253
ISSN: 1874-4400

RESEARCH ARTICLE **OPEN ACCESS**

A Hybrid Image Denoising Framework using Adaptive Clustering and Residual Analysis

Archana Saini[1,*] and Ayush Dogra[2]

[1]*Department of Computer Science Engineering, Chitkara University Institute of Engineering Technology, Chitkara University, Rajpura, Punjab, 140401, India*
[2]*Department of Electronics and Communication Engineering, Chitkara University Institute of Engineering Technology, Chitkara University, Rajpura, Punjab, 140401, India*

Abstract:

Introduction: Image denoising is an important preprocessing step in medical imaging, reducing noise while preserving essential structural information. But existing denoising methods exhibit inconsistent performance across different imaging modalities and noise levels.

Methods: Experiments are performed on HRCT and MRI data corrupted with Gaussian noise at various noise levels (low to high). A hybrid approach has been proposed by using the method of noise concept. This study also presents a comparative evaluation of various image denoising techniques using both reference and non-reference metrics.

Results: Experimental results demonstrate that the proposed method exhibits consistent, symmetric degradation in PSNR and SSIM as the noise level increases. For dataset1, the proposed method achieves a PSNR of 31.62 and 24.98 at noise levels of 10 and 40, respectively. Similarly, for dataset2, the PSNR is 36.54 at noise level 10 and 28.68 at 40.

Discussion: Although several denoising methods have been proposed, most perform well only in low-noise conditions, with performance improving as the noise level decreases. Based on both reference-based (PSNR, SSIM, and entropy) and no-reference perceptual quality features (NIQE, BRISQUE, and PIQE), the research provides an in-depth comparative study of various filters, bilateral filter variants, and advanced hybrid denoising methods. One of the primary strengths of the proposed method is its superior performance at high noise levels.

Conclusion: These results indicate the effectiveness and reliability of the proposed method for denoising high-quality images, particularly in challenging high-noise scenarios. The quantitative and perceptual quality results show that it is an effective preprocessing tool for medical imaging.

Keywords: ACPT, Gaussian noise, HRCT, Hybrid, Image denoising, MRI, PSNR.

© 2026 The Author(s). Published by Bentham Open.
This is an open access article distributed under the terms of the Creative Commons Attribution 4.0 International Public License (CC-BY 4.0), a copy of which is available at: https://creativecommons.org/licenses/by/4.0/legalcode. This license permits unrestricted use, distribution, and reproduction in any medium, provided the original author and source are credited.

*Address correspondence to this author at the Department of Computer Science Engineering, Chitkara University Institute of Engineering Technology, Chitkara University, Rajpura, Punjab, 140401, India;
E-mail: saini.archana@chitkara.edu.in

Cite as: Saini A, Dogra A. A Hybrid Image Denoising Framework using Adaptive Clustering and Residual Analysis. Open Neuroimaging J, 2026; 19: e18744400493253. http://dx.doi.org/10.2174/0118744400493253260715094516

Received: February 13, 2026
Revised: May 04, 2026
Accepted: May 12, 2026
Published: July 17, 2026

Send Orders for Reprints to
reprints@benthamscience.net

1. INTRODUCTION

Image denoising is a fundamental task in image processing and computer vision that seeks to reconstruct a clean, interference-free image from noisy or otherwise degraded observations [1]. Gaussian noise has been the most studied noise model, utilised in a wide variety of real-world imaging applications and possessing mathematically well-behaved properties. Gaussian noise significantly degrades perceptual image quality, further degrading performance on tasks such as segmentation, classification, and recognition. A wide range of methods have been developed to address Gaussian noise over time, from spatial-filtering-based models to more recent learning-based models. Early approaches were based on spatial-domain filters, such as the Gaussian and bilateral filters, which smooth noise but often degrade the fine details of an image [2]. The above improvements in results have been achieved using adaptive filtering approaches that adjust the level of smoothing based on local image characteristics [3]. Standard filtering methods, *e.g.*, median, Wiener, and Gaussian filters, have been compared across different Gaussian noise standard deviations, and the results have been found to depend heavily on the noise standard deviation [4].

Non-local means and variational approaches performed better at denoising by leveraging image self-similarity and statistical priors [5]. Also, probabilistic modelling of noise using mixed Poisson-Gaussian models has increased the utility of denoising techniques in low-light and medical imaging environments. Recent advances in machine learning and deep learning have achieved remarkable improvements in robustness to varying noise intensity by enabling adaptive estimation of noise maps across different values of $\boldsymbol{\sigma}$ [6].

Over the past few years, hybrid image denoising has emerged as a promising research direction, aiming to combine the strengths of multiple denoising paradigms while mitigating the shortcomings of individual methods. For example, techniques that integrate spatial filtering with wavelet- or transform-domain shrinkage have demonstrated improved noise reduction while preserving fine details [7]. Such hybridization methods are particularly effective against Gaussian noise across various sigma levels, owing to their ability to leverage complementary properties.

Recent trends in image denoising have focused more on hybrid approaches and deep learning-based feature extraction. To achieve better feature extraction and motion-aware detection in more complex scenarios, hybrid recursive neural network models together with optimization methods have been proposed [8]. In medical imaging, attention-based encoder-decoder architectures, such as enhanced U-Net models, have demonstrated improved feature representation and structural preservation [9].

Also, recent survey research on denoising shows the extent to which deep learning methods simulate the underlying noise distribution and hierarchical features of medical images. These methods improve denoising performance over traditional methods by applying convolutional, recurrent, and attention principles [10].

These methods usually require extensive annotated datasets, lengthy training, and expensive computational resources despite their excellent results. The proposed framework focuses on a non-learning-based hybrid approach that does not rely on training data, offering a computationally efficient alternative while maintaining competitive denoising performance.

1.1. Contribution

- A new hybrid denoising model is developed to reduce Gaussian noise across different noise levels.
- Its structure involves ACPT-based denoising, then the method noise is calculated, and residual features are extracted using it.
- A co-occurrence filter is also applied to the residual features in order to increase structural agreement and minimise correlated noise elements.
- The increased residuals are processed in terms of wavelet decomposition and BayesShrink thresholding, and the wavelet image reconstruction is carried out.
- Lastly, the denoised image is obtained by taking an effective middle-ground between the reconstructed wavelet and the ACPT-denoised output.

2. RELATED WORK

In a previous study [11], the authors proposed an adaptive filtering method that achieves optimal noise reduction while preserving high-spatial-frequency detail. The adaptive threshold is flexible and changes with the amount of noise. The Adaptive Weight Function (AWF) is used in dissimilarity measurement, which relies on the spatial distance between the reference patch and the candidate patches. It has been tested on various digital images and demonstrates significant improvements in visual quality, as well as PSNR and SSIM scores. In another study [12], researchers improved block-matching and 3D filtering (BM3D) image denoising by enhancing noise-variance estimation, domain-transform filtering, and nonlinear filtering. They proposed multilayer wavelet decomposition for noise-variance estimation, compressive-sensing-based Gaussian-sequence Hartley-domain transform filtering, and edge-preserving smoothing. In a related study [13], the authors presented a new bitonic filter, a non-learning-based method that employs mathematical morphology and is adapted to local signal properties. It achieved significant noise-reduction benefits without increasing processing. With optimal training, the bitonic filter achieves a signal-to-noise ratio that is only 2.4dB worse than that of state-of-the-art learning-based methods. Still, the difference is higher with adapted training images. A hybrid approach to designing a medical image denoising filter based on bio-inspired optimisation algorithms was presented [14]. This algorithm is a Hybrid of Cuckoo Particle Swarm Optimisation (HCPSO) and a Guided Decimation Box Filter (GDBF). The filter's

performance is compared with that of other bio-inspired genetic algorithms. It achieves the best values for PSNR, SSIM, and FSIM, demonstrating its effectiveness in numerical and visual quality.

A hybrid solution based on an adaptive Kalman filter to reduce noise, the Non-Local Means (NLM) method, and a median filter to sharpen the denoised image was presented [15]. The parameters can be optimised using a Latin square. The experimental findings indicate that noise reduction and image feature conservation are significantly enhanced. In a further study [16], researchers introduced a new method to remove white noise as a component of Gaussian noise. This technique applies to both similar and dissimilar patches, and detects inter-correlations between dissimilar pixels. The technique's performance demonstrates that it is much faster than other noise-removal algorithms. A study [17] investigated the noise-reduction parameters of BM3D filtering algorithms using a complex network conglomeration model and an ANN. The experimental findings show a high PSNR of 51.94 and an SSIM of 0.998.

Researchers proposed [18] a hybrid image denoising algorithm that combines wavelet transforms with deep learning methods. The wavelet transform is applied to decompose the image into various frequency components. The approximation coefficients are then denoised using a dedicated CNN. The experimental outcomes demonstrate that this hybrid method is more efficient than conventional denoising techniques. Previously, authors presented [19] a hybrid denoising algorithm that combines the Adaptive Median Filter (AMF) and the Modified Decision-Based Median Filter (MDBMF) to enhance image quality and structural integrity. The quantitative tests indicate better PSNR, IEF, MSE, SSIM, FOM, and VIF, with improvements of up to 0.07 and 0.68, respectively. In a related study [20], the authors used a denoising method that estimates each pixel’s value using the weighted average of its surrounding pixels. This weight may be termed MSE-Weight. The weight of the centre pixel in the neighbourhood (CW) is selected and carefully designed in the two-step pre-filtering and denoising process of the proposed method. The proposed approach achieves an average 0.80 dB higher mean Peak Signal-to-Noise Ratio (PSNR) and a 0.0239 improvement in SSIM.

The Rolling Guidance Filter (RGF) is a smoothness-based method designed to remove small-scale features, such as noise or texture, in an image without eliminating significant edges [21]. Large edges that would otherwise be lost in a single-pass bilateral filtering process can be progressively restored by the method, which repeatedly applies a bilateral filter as the guiding image is re-estimated at each step. This rolling mechanism improves structural consistency and effectively separates texture removal from edge preservation. A study [22] proposed a fast bilateral filtering method, based on Fourier kernel approximations, in order to address the high computational complexity of traditional bilateral filters. By reformulating the nonlinear range kernel using a truncated Fourier series, the authors could represent the bilateral filter as a weighted sum of linear convolutions. The proposed approach significantly reduces execution time, and the estimate accuracy is close to that of the exact solution.

In another study [23], the authors proposed a denoising system that used Gaussian and bilateral filtering along with a noise-thresholding method. The output of this approach is a preliminary denoised image produced using a Gaussian or bilateral filter. The difference between the noisy and filtered images (the residual) is then processed using a thresholding method to remove noise while retaining important details. While noise thresholding is useful for extracting fine image features, the bilateral filter component ensures that edges are preserved. This work has shown that combining spatial filtering and residual-domain processing enhances image denoising.

The concept of method noise thresholding to the Non-Local Means (NLM) filtering model was generalized in a study [24]. The proposed algorithm initially applies NLM filtering to exploit non-local self-similarity to minimise noise, and then thresholds the residual noise to enhance the denoised image. The algorithm outperformed bilateral filtering and conventional NLM, particularly in textured regions. In a subsequent study [25], the authors proposed a fast and accurate bilateral filtering method that, by theory, guarantees a bound on the approximation error. The proposed method converts a sequence of linear filtering operations into a nonlinear bilateral filter by using a polynomial approximation of the range kernel. This approach offers greater control accuracy at a lower computational cost than heuristic acceleration. The methodology faithfully reproduces the exact bilateral filter output and provides significant speedups. In another study [26], the authors provided a robust bilateral filtering process using optimally weighted kernels computed with the Stein Unbiased Risk Estimator (SURE). The method enhances denoising across a range of noise levels by adaptively selecting optimal filter settings to minimize mean squared error. The approach enhances robustness and reduces parameter sensitivity by incorporating statistical risk estimation into the bilateral filtering model. In a later study [27], researchers presented an image denoising framework based on score-based diffusion probabilistic models (DDPMs). By learning the score function of the data distribution, image denoising can gradually remove noise and can be formulated as a generative reverse diffusion process. Two complex noise features in PET imaging that the model has well represented are low-count noise and spatially varying deterioration.

A new optimal deep convolutional neural network-based vectorial variation (ODCNN) filter for denoising medical Computed Tomography (CT) images and the Lena images was introduced [28]. It implements a noisy-pixel-map identification module executed by a deep CNN trained with the Adam algorithm. Upon detecting noisy pixels, a noise removal module is invoked, based on the FAT and Lion algorithms, specifically the Feedback Artificial Lion (FATL) optimization algorithm. Afterwards,

pixel enhancement is performed using the vectorial total variation norm, which then produces the final enhanced image. The proposed FAL algorithm achieves the best performance, with a PSNR of 24.149 dB, a Second-Derivative-like Measure of Enhancement (SDME) of 32.142 dB, a structural similarity index (SSIM) of 0.800, and an Edge Preserve Index (EPI) of 0.9267, outperforming existing techniques. A bio-inspired optimization filtering system, named the Bilateral Filter (BF), was proposed for MI denoising [29]. The optimal Gaussian and spatial weighting parameters are selected using swarm-based optimization techniques, namely the Dragonfly (DF) and Modified Firefly (MFF) algorithms, through a multi-objective fitness function that incorporates PSNR and VRMSE. A Convolutional Neural Network (CNN) classifier is employed to classify the denoised images as normal or abnormal, achieving a PSNR of 47.52 dB and an error rate of 1.23, outperforming existing filters and classifiers.

3. PRELIMINARIES

3.1. Adaptive Clustering and Progressive PCA Thresholding (ACPT)

This is an image denoising method that involves detail preservation. This approach is intended to address one of the central issues in Gaussian denoising: suppressing noise while minimizing loss of fine structures and edges. The approach described as the ACPT has two basic steps:

3.1.1. Adaptive Clustering

The image patches are combined into clusters based on similarity, enabling the same algorithm to leverage local redundancy. This dynamic clustering provides different structures in pairings and makes the noise extraction more resistant. Compared with fixed clustering, ACPT does not assume or predetermine cluster size or membership; instead, these are dynamically adjusted based on the local noise level and image content.

3.1.2. Progressive Principal Component Analysis (PCA) Thresholding

Principal Component Analysis (PCA) is used in each cluster to rotate correlated patches into a decorrelated domain. A progressive threshold is then applied to the PCA coefficients, using a hard threshold for elements dominated by noise and a soft threshold for elements with structural information. The effect of this progressive mechanism is to preserve fine image details, such as edges and textures, and to prevent over-smoothing.

3.2. Co-occurrence Filter

A Co-occurrence Filter (CoF) is a nonlinear filtering method that utilizes statistical correlations between pixel intensities to smooth the image, remove noise, and preserve edges. CoF leverages co-occurrence statistics within a two-level abstraction structure to determine how to smooth the pixels. A co-occurrence matrix is extracted based on the image that corresponds to the frequency of the pixel values that occur in relation to each other within a given local area. Such a matrix stores contextual data by representing not only the similarity between pairs of pixels but also the spatial distribution of intensity relationship patterns within the image. The weight is assigned by the filter to pixel pairs on the basis of co-occurrence frequency. Frequently, co-occurring pixels tend to belong to a similar region or structure, and consequently, they are averaged more strongly. On the other hand, pixels with rare co-occurrence values are most likely to reside in other regions and will receive lower weights, thereby preserving sharp transitions. Based on the co-occurrence matrix, the weighted average of the neighbouring pixels is set to replace the original pixel.

3.3. Wavelet Decomposition

The noisy image can be decomposed into bands of high-frequency details and low-frequency sub-bands. The main targets of the denoising attacks are the high-frequency bands.

3.4. BayesShrink Thresholding

BayesShrink employs a Bayesian formulation that computes thresholds adapted to each sub-band. The balance phenomenon, which reduces noise while preserving coefficients, improves the threshold and thereby reduces the Bayesian risk. BayesShrink adapts to changes in signal-to-noise ratio across sub-bands, unlike universal or fixed thresholds.

3.5. Wavelet Reconstruction

The noisy image is restored with the inverse wavelet transform after using the thresholding.

4. PROPOSED METHODOLOGY

The proposed architecture includes the Adaptive Clustering with Progressive PCA Thresholding (ACPT) denoising method [30].

In ACPT, image patches are grouped based on similarity to exploit non-local redundancy. Initially, patches are over-clustered using K-means. The number of clusters is defined as in Eq. (**1**):

$$K = \max\left(\frac{ab}{256^2}, 4\right) \quad \textbf{(1)}$$

where a x b denotes the image size.

The similarity between clusters is defined using the Euclidean distance between their mean vectors using Eq. (**2**):

$$\| y_A - y_B \|_2^2 \quad \textbf{(2)}$$

Two clusters are merged by using Eq. (**3**) if:

$$\| y_A - y_B \|_2^2 < T \quad \textbf{(3)}$$

where the threshold is given in Eq. (**4**):

$$T = 16\sigma^2 \quad \textbf{(4)}$$

This adaptive merging ensures that structurally similar patches are grouped while accounting for noise variance.

For each cluster, a patch matrix X is formed and decomposed using singular value decomposition using Eq. (**5**):

$$X = U\Sigma V^T \quad \textbf{(5)}$$

The progressive thresholding consists of two stages, hard and soft thresholding, as given in Eqs. (**6**, **7**, and **8**), respectively:

4.1. Hard Thresholding (MP-based)

$$\tilde{X} = \sum_i \sqrt{\lambda_i} \cdot \mathbf{1}\left(\sqrt{\lambda_i} > \xi\right) \cdot u_i v_i^T \quad \textbf{(6)}$$

where the threshold is defined as:

$$\xi = \sqrt{\mu\lambda_{n+}}, \lambda_{n+} = \sigma^2(1+\sqrt{\gamma})^2 \quad \textbf{(7)}$$

Here, σ is the noise standard deviation and γ is the patch dimensionality ratio.

4.2. Soft Thresholding (LMMSE refinement)

$$s_i = \max\left(\frac{S_i - \sigma^2}{S_i}, 0\right) s_i \quad \textbf{(8)}$$

where S_i represents the local variance of coefficients.

The denoising procedure by ACPT is summarized as follows:

Input: Noisy image Y, noise level σ

Output: Denoised image $\hat{X}$

1. Patch Extraction:

Extract overlapping patches from Y and vectorize each patch.

2. Adaptive Clustering:

a. Perform initial over-clustering using K-means with a large number of clusters.

b. Iteratively merge clusters whose mean distance satisfies:

$||y_A - y_B||^2 < T$, where $T = 16\sigma^2$.

3. For each cluster:

a. Construct data matrix X from grouped patches.

b. Compute SVD: $X = U\Sigma V^T$.

c. Hard Thresholding (MP-based):

Retain singular values where:

$\sqrt{\lambda_i} > \xi$,

where $\xi = \sqrt{(\mu\lambda_{n_+})}$, and $\lambda_{n_+} = \sigma^2(1 + \sqrt{\gamma})^2$.

d. Soft Thresholding (LMMSE):

Apply shrinkage:

$\hat{s}_i = \max((S_i - \sigma^2)/S_i, 0) \cdot s_i$

4. Patch Aggregation:

Reconstruct denoised patches and aggregate them using weighted averaging.

5. Image Reconstruction:

Combine all patches to form the final denoised image $\hat{X}$.

The proposed denoising procedure is summarized as follows:

1. Read the original image I.
2. Add Gaussian noise with standard deviation σ to obtain:
   $I_n = I + N(0,\sigma^2)$
3. Apply the Adaptive Clustering Patch Transform (ACPT) to the noisy image:
   $I_{ACPT} = \text{ACPT}(I_n,\sigma)$
4. Compute the method noise as the difference between the noisy image and the ACPT output:
   $MN = I_n - I_{ACPT}$
5. Extract residual features by subtracting the denoised image from the method noise:
   $RF = MN - I_{ACPT}$
6. Apply a Co-occurrence Filter (CoF) to the residual feature image:
   $I_{CoF} = \text{CoOccurrenceFilter}(RF, \text{filter_size}, \sigma)$
7. Perform a multi-level 2D Discrete Wavelet Transform (DWT) on the method noise using a Daubechies wavelet:
   $\{C,S\} = \text{DWT}(MN)$
8. Apply BayesShrink thresholding to each high-frequency subband:
   $\hat{C}_i = \text{BayesShrink}(C_i)$
9. Reconstruct the filtered residual image using inverse DWT:
   $I_{WT} = \text{IDWT}(\hat{C})$
10. Combine the ACPT output and wavelet-reconstructed residual:
    $I_{rec} = I_{ACPT} + I_{WT}$
11. Fuse the ACPT-denoised image and the reconstructed image *via* averaging:
    $I_f = \frac{I_{ACPT} + I_{rec}}{2}$

Figure 1 shows the proposed methodology, which takes a noisy image contaminated by Gaussian noise as input. All subsequent operations aim to maintain anatomical features (textures, edges) and to separate significant image structures from noise. The ACPT image denoising method is first used on the noisy image. This operation is a robust base-de-noise. The difference between the ACPT output and the noisy image is taken as a measure of the method's noise.

This idea is inspired by residual extraction: what is removed rather than what is retained. To obtain residual characteristics, the noise technique is further processed. Noise and small-scale elements occupy similar frequency bands, which the framework explicitly models rather than rejecting. To isolate structured patterns (real texture) and random noise, the residual feature image is passed to a co-occurrence analysis block to co-vary pixel intensities with their neighbours. The co-occurrence-refined residual is then wavelet-decomposed. The image is decomposed into two components: detail components (textures and edges) and approximation components (low-frequency structure). The informative coefficients are preserved by selectively applying thresholding. Spatial domain reconstruction is performed using the computed wavelet coefficients. The final output is obtained by adding the ACPT output to the reconstructed image.

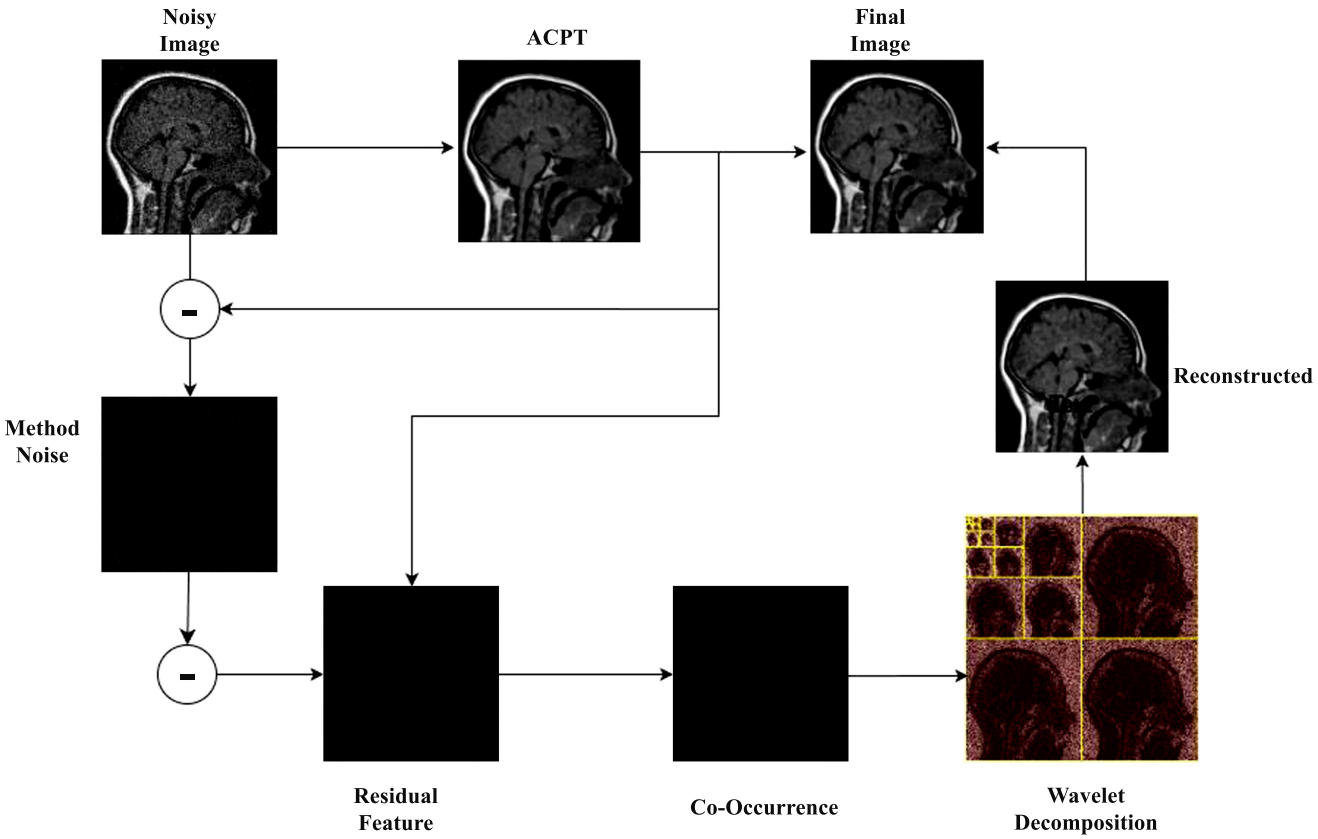

Fig. (1). Working of the proposed methodology.

The sequence of the proposed framework is developed through a staged refinement method. ACPT is initially applied to remove Gaussian noise without relying on significant structures, using adaptive clustering and PCA-based thresholding. The residual (method-noise) is then recovered to isolate the content removed in this initial denoising stage, which includes both noise and small structural features. To allow targeted denoising, the residual is treated independently and is no longer simply subject to further filtering.

To distinguish between organized patterns (like edges and textures) and uncorrelated noise, a co-occurrence filter is then applied to the residual to exploit statistical dependencies between neighboring pixels. This process improves the structural consistency of the residual domain. Wavelet-based thresholding is employed to obtain multi-scale noise suppression. The reason is that wavelet decomposition is effective at removing high-frequency noise without losing important image data. This ordered pipeline is followed so that high noise is removed first, followed by the refinement of structured details.

5. EXPERIMENTAL SETUP

HRCT and MRI are the two imaging modalities used in the experiment. The dataset is accessible to the general public and is open source [31]. The dataset images are stored in .png format with 8-bit depth and a spatial resolution of 256 × 256 pixels. The images in the repository are clean (noise-free) images, and no paired noisy-clean ground truth is provided. Therefore, synthetic Gaussian noise is added to the images at different standard deviation levels (σ = 10, 20, 30, and 40) to allow for controlled quantitative evaluation. Figure **2a** shows chest HRCT, and Figure **2b** shows a T1-weighted MRI sequence. All experiments are implemented in MATLAB on a PC equipped with an AMD Ryzen 3-3250U processor (2.6 GHz) and 4 GB of RAM. Table **1** demonstrates the parameter settings of the Proposed Method.

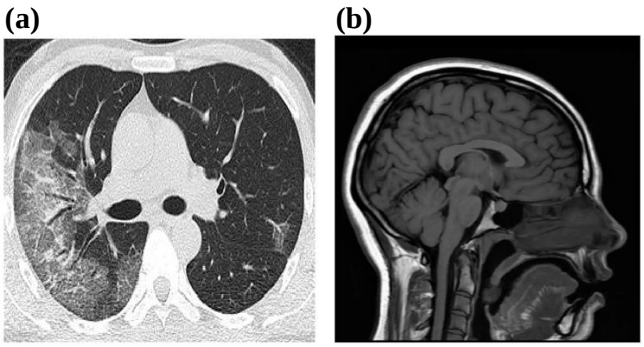

Fig. (2). (**a**) Dataset1(HRCT image), (**b**) Dataset2(MR image) [31].

Table 1. Parameter settings of the proposed method.

Component	Parameter	Description
ACPT	Patch size	8 × 8
	Number of clusters (K)	$K=\max(ab/256^2, 4)$
	Clustering method	K-means (over-clustering + merging)
	Merging threshold	$T = 16\sigma^2$
	PCA threshold parameter (μ)	1.1
	Noise estimation	Blind estimation (wavelet-based MAD)
Wavelet	Wavelet type	Daubechies (db4)
	Decomposition level	3
	Thresholding method	BayesShrink
	Threshold type	Subband adaptive
	Reconstruction	Inverse DWT (IDWT)
CoF	Filter size	Adaptive (proportional to σ)
Fusion	Weight	0.5 (linear averaging)

6. RESULTS AND DISCUSSION

Tables 2 and 3 present the visual results of different image denoising algorithms for datasets 1 and 2 at various noise levels. To evaluate the different filtering and denoising methods quantitatively on datasets 1 and 2 across increasing noise levels, entropy, PSNR, SSIM, and no-reference image quality measures (NIQE, BRISQUE, and PIQE) were used. The corresponding results are shown in Tables 4 and 5.

Table 4 shows that filters such as rolling guidance, Gaussian, median, and bitonic have high entropy values, indicating that they preserve texture better. Specifically, the minimum SSIM of Rolling Guidance is low at low noise levels and at PSNRs below 15 dB, indicating that structural fidelity is low despite the smoothing. The bitonic, Gaussian, and median filters demonstrate that they are insufficient under high-noise conditions, as they only marginally improve SSIM and offer limited noise-reduction capability.

The GBFMT and NLFMT methods achieve a significant increase in PSNR compared with traditional filters, with PSNR values exceeding 28 dB at low noise ($\boldsymbol{\sigma} = 10$). Their SSIM value, however, is extremely low (0.15), indicating that noise reduction is effective but that structural information is not properly preserved. Moreover, both methods exhibit a monotonic decrease in PSNR with increasing noise and are sensitive to increases in noise variance. The Fast Bilateral Filter V2 yields good SSIM and PSNR at low noise levels; at $\boldsymbol{\sigma} = 10$, SSIM exceeds 0.86, and PSNR is approximately 29.76 dB. But the higher the noise level, the faster performance decreases and SSIM drops below 0.1. This implies that noise levels are high in rapid bilateral approximations. The Robust Bilateral Filter yields higher SSIM values and more stable PSNR, and thus remains more successful across all noise levels compared to fast bilateral variants. It is also rated lower on BRISQUE and PIQE, which are superior in terms of perceived quality and artifacts. In this setting, the Fast and Accurate Bilateral Filter performs well, with average SSIM and PSNR, but as the noise level increases, the perceptual measures degrade. eBM3D exhibits moderate denoising performance, with PSNR values from 27.64 dB to 21.56 dB as noise increases, and SSIM values dropping from 0.74 to 0.50. BRISQUE values range from 5.76 to 6.29, with NIQE and PIQE increasing, indicating degraded perceptual quality. While eBM3D effectively suppresses noise, it loses fine details at higher noise levels. In contrast, the proposed method shows improved structural preservation and perceptual quality, reflected in higher SSIM values and better visual consistency across noise levels. OD-CNN performs fairly consistently across all noise levels, as shown by PSNR values ranging from 27.45 dB to 20.02 dB and SSIM values ranging from 0.79 to 0.61. It also shows good structure preservation even at higher noise levels. Also, perceptual quality measurements like BRISQUE and NIQE, which stay within reasonable limits, suggest that the visual quality is good. BF-CNN, on the other hand, has much lower SSIM (from 0.60 to 0.50) and PSNR (from 23.53 dB to 17.22 dB), indicating that it doesn't preserve the structure as well. Also, BF-CNN has higher BRISQUE and PIQE values, indicating that perceived quality is degrading, especially in the presence of more noise. The reference-based and no-reference measures have shown that ACPT is the best among the examined methods. It works even better when noise is increased, achieving the highest PSNR (31.60 dB) and SSIM (0.8918) at $\boldsymbol{\sigma} = 10$. The proposed ACPT-based approach also improves performance, yielding lower NIQE and BRISQUE values and the highest SSIM across all noise levels.

Table 2. Visual results for dataset 1.

Algorithms	Noise Levels			
	10	20	30	40
Rolling Guidance	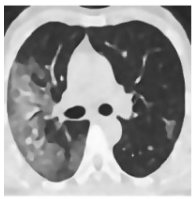	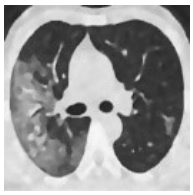	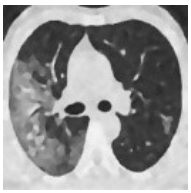	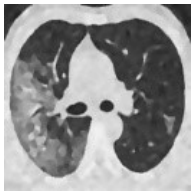
Bitonic	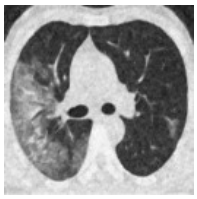	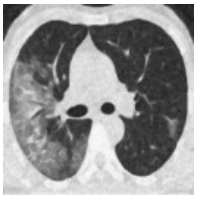	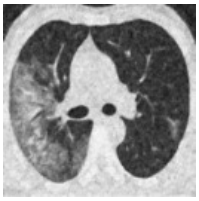	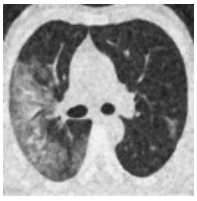
Gaussian	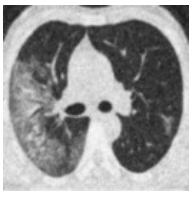	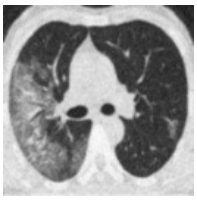	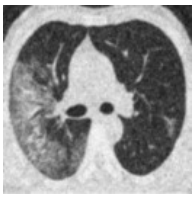	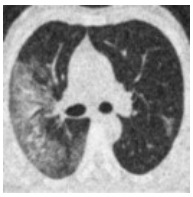
Median	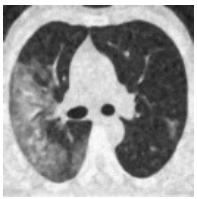	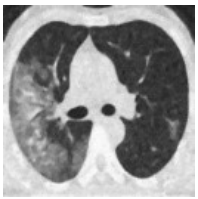	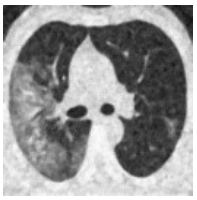	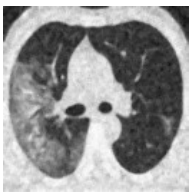
GBFMT				
NLFMT				
SDPM				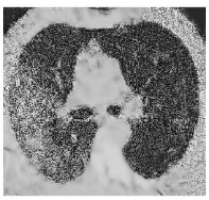

(Table 2) contd.....

Algorithms	Noise Levels			
	10	20	30	40
eBM3D				
FastBilateralV2				
Robust Bilateral				
FastAccurateBilateral			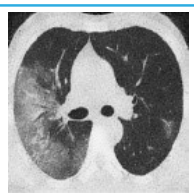	
OD-CNN				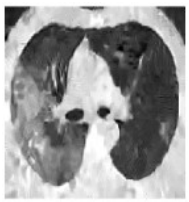
BF-CNN		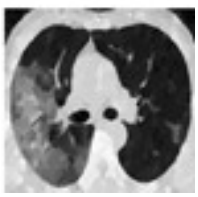		
ACPT				
Proposed				

Table 3. Visual results for dataset 2.

Algorithms	Noise Levels			
	10	20	30	40
Rolling Guidance	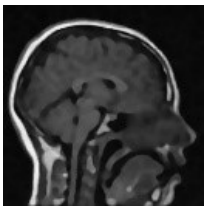	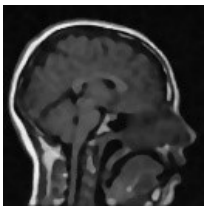	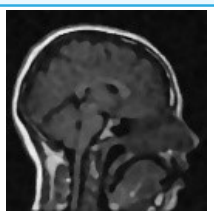	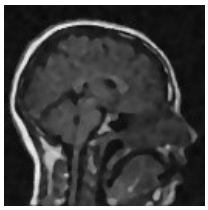
Bitonic	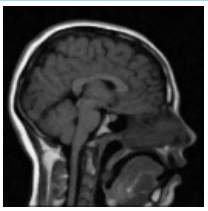	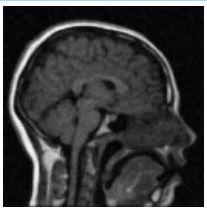	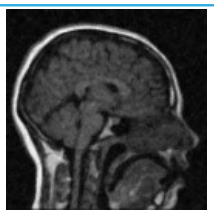	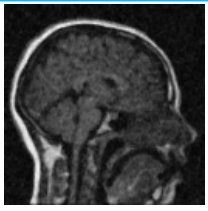
Gaussian	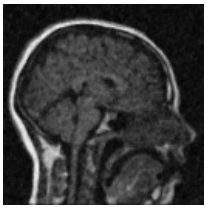	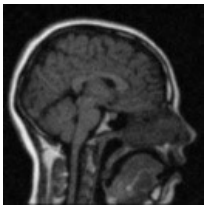	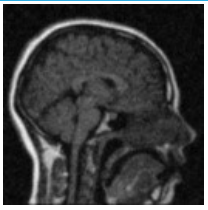	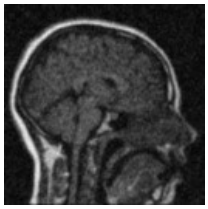
Median	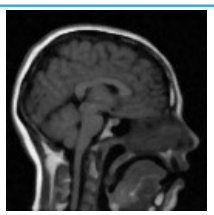	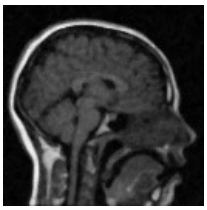	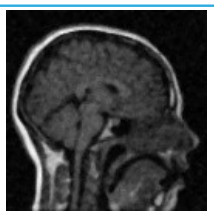	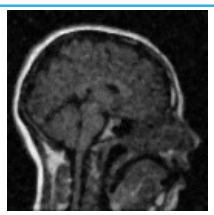
GBFMT	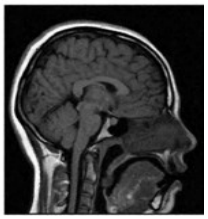			
NLFMT	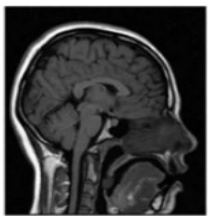	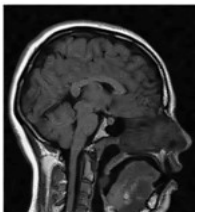	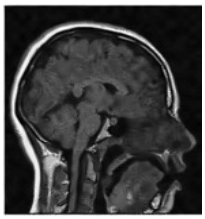	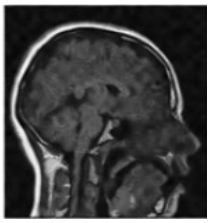
SDPM	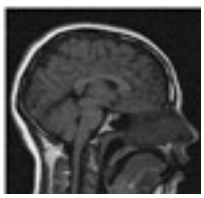		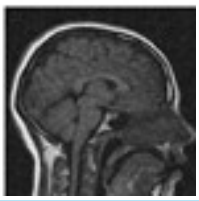	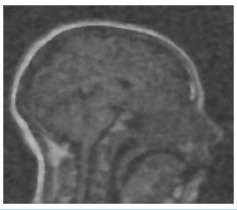

(Table 3) contd.....

Algorithms	Noise Levels			
	10	20	30	40
eBM3D	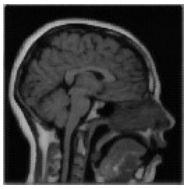	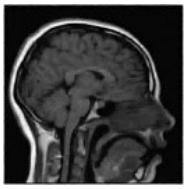	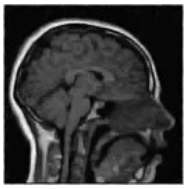	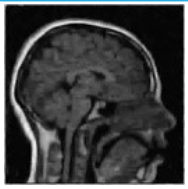
FastBilateralV2	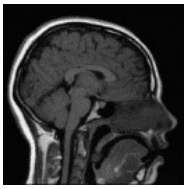	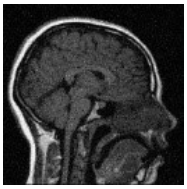		
Robust Bilateral	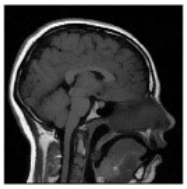	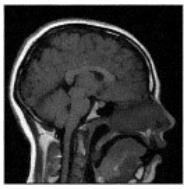	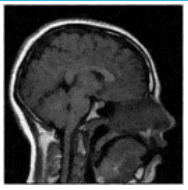	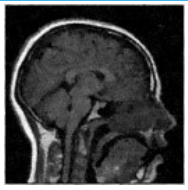
FastAccurateBilateral	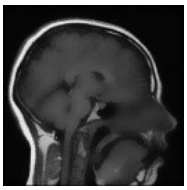	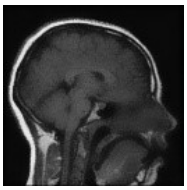	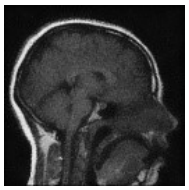	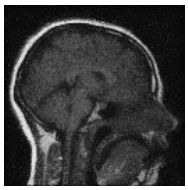
OD-CNN		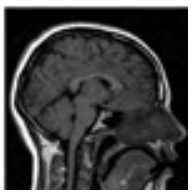	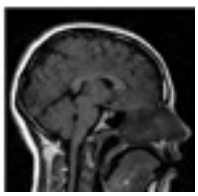	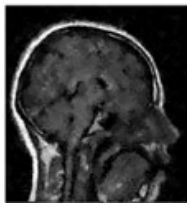
BF-CNN		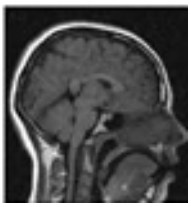	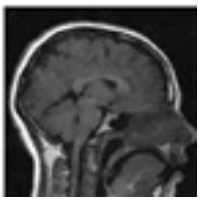	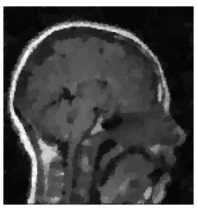
ACPT	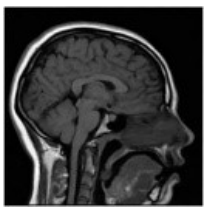	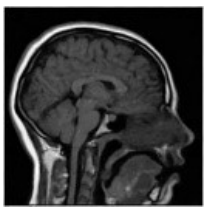	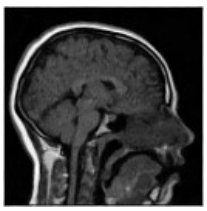	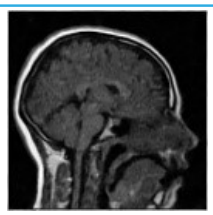
Proposed	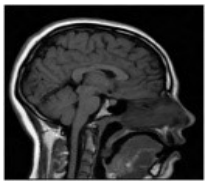		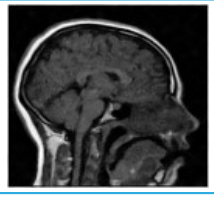	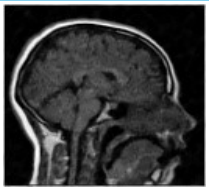

Table 4. Performance metrics-based result for dataset 1.

Dataset 1	-	Entropy	PSNR	SSIM	NIQE	BRISQUE	PIQE
Rolling Guidance	10	6.79	14.65	0.03	5.68	31.10	44.73
	20	6.91	14.30	0.32	14.14	42.45	62.92
	30	6.92	13.86	0.32	16.73	46.72	68.21
	40	6.93	13.41	0.31	24.48	48.55	76.02
Bitonic	10	7.24	5.67	0.30	5.78	38.57	25.62
	20	7.18	5.69	0.31	6.52	37.02	36.87
	30	7.29	5.93	0.29	5.79	40.89	26.98
	40	7.29	5.98	0.29	5.79	40.89	26.98
Gaussian	10	7.26	5.76	0.30	7.45	36.79	54.36
	20	7.22	5.77	0.31	8.01	39.33	61.14
	30	7.28	6.04	0.29	7.16	38.68	47.99
	40	7.28	6.09	0.29	7.16	38.68	47.99
Median	10	7.34	5.60	0.30	7.94	42.34	14.60
	20	7.23	5.67	0.31	7.59	42.84	19.21
	30	7.44	5.77	0.28	8.35	41.64	13.55
	40	7.44	5.82	0.28	8.35	41.64	13.55
GBFMT	10	3.21	28.39	0.14	4.61	45.88	32.06
	20	3.28	22.55	0.14	4.22	45.33	25.87
	30	3.30	19.31	0.14	4.10	44.67	24.81
	40	3.30	17.11	0.15	4.00	44.47	24.62
NLFMT	10	3.25	28.38	0.14	6.09	47.83	45.99
	20	3.30	22.54	0.14	4.62	46.50	32.51
	30	3.27	19.31	0.15	3.81	45.55	29.54
	40	3.25	17.12	0.15	4.47	46.16	30.75
SDPM	10	6.70	23.19	0.69	3.66	30.60	34.15
	20	6.88	22.55	0.63	4.19	30.08	31.32
	30	6.78	21.11	0.60	5.12	36.09	30.27
	40	6.00	18.07	0.57	4.40	33.46	31.27
eBM3D	10	7.19	27.64	0.74	5.76	37.58	37.06
	20	7.26	24.47	0.61	5.82	39.81	51.17
	30	7.35	22.86	0.54	6.29	40.03	58.99
	40	7.41	21.56	0.50	6.13	40.79	58.04
FastBilateralV2	10	7.35	29.76	0.86	7.44	25.69	40.22
	20	7.68	14.32	0.14	14.47	41.25	61.45
	30	7.73	13.65	0.10	16.83	47.09	67.86
	40	7.71	12.98	0.08	23.23	47.35	70.94
Robust Bilateral	10	7.18	29.36	0.85	7.44	22.28	24.41
	20	7.24	26.88	0.74	7.74	27.33	24.01
	30	7.23	25.59	0.68	8.89	28.59	18.41
	40	7.29	24.49	0.64	7.49	31.83	13.72
FastAccurateBilateral	10	6.87	25.31	0.69	5.79	11.65	18.98
	20	7.17	15.06	0.25	13.06	32.69	43.49
	30	7.42	14.75	0.18	19.29	40.01	59.62
	40	7.54	14.25	0.13	25.56	44.01	65.33
OD-CNN	10	7.01	27.45	0.79	4.16	25.90	29.99
	20	7.00	23.67	0.73	4.13	25.87	27.70
	30	6.95	21.80	0.66	4.84	26.37	26.10
	40	6.56	20.02	0.61	5.10	30.78	28.15
BF-CNN	10	5.941	23.536	0.60	6.17	44.75	56.62
	20	5.469	21.549	0.55	5.97	44.51	57.77
	30	5.521	18.591	0.52	4.58	45.39	51.80
	40	5.093	17.220	0.50	5.74	43.45	52.85
ACPT	10	7.26	31.60	0.89	6.04	24.00	25.95
	20	7.22	28.04	0.78	5.56	18.88	19.47
	30	7.23	26.19	0.70	4.70	30.68	22.28
	40	7.21	24.93	0.63	5.83	38.25	23.31
Proposed	10	7.27	31.62	0.89	5.33	23.93	26.01
	20	7.23	28.07	0.79	4.65	19.18	22.50
	30	7.27	26.23	0.71	4.75	26.28	22.76
	40	7.28	24.98	0.65	5.61	37.27	22.46

Table 5. Performance metrics-based results for dataset 2.

Dataset 2 (MRI)	-	Entropy	PSNR	SSIM	NIQE	BRISQUE	PIQE
Rolling Guidance	10	6.91	15.53	0.07	5.77	49.13	85.22
	20	6.49	15.57	0.08	6.26	46.07	79.50
	30	6.53	15.60	0.08	6.42	48.21	78.56
	40	6.57	15.57	0.09	6.64	49.48	81.13
Bitonic	10	6.67	5.65	0.60	5.30	42.53	60.28
	20	6.67	5.59	0.53	6.05	43.14	43.52
	30	6.74	5.74	0.47	6.20	42.43	33.25
	40	6.79	5.74	0.43	6.61	41.73	32.62
Gaussian	10	6.59	5.74	0.60	6.89	43.38	81.17
	20	6.69	5.66	0.52	7.48	43.33	66.99
	30	6.76	5.84	0.47	7.35	43.02	59.84
	40	6.79	5.84	0.42	7.52	42.66	49.86
Median	10	6.56	5.59	0.60	7.35	42.17	52.30
	20	6.72	5.58	0.53	7.08	43.66	28.44
	30	6.79	5.60	0.49	8.34	43.98	26.59
	40	6.84	5.60	0.44	8.71	41.50	15.60
GBFMT	10	3.00	29.01	0.07	3.73	46.21	43.97
	20	3.08	23.16	0.07	4.36	46.14	36.63
	30	3.13	19.81	0.06	4.48	45.58	34.12
	40	3.15	17.52	0.06	4.59	45.31	33.50
NLFMT	10	3.01	28.98	0.07	7.55	49.17	40.98
	20	3.03	23.13	0.07	6.35	50.26	46.50
	30	3.08	19.79	0.07	6.45	49.80	51.09
	40	3.10	17.50	0.08	6.44	49.47	49.23
SDPM	10	5.99	28.28	0.81	5.78	53.01	64.14
	20	6.22	26.45	0.77	5.88	48.43	64.74
	30	5.24	23.85	0.74	5.99	54.17	68.09
	40	5.82	23.65	0.81	6.14	45.46	65.00
eBM3D	10	6.63	33.26	0.87	4.35	38.77	66.40
	20	6.62	29.12	0.80	4.21	37.09	79.30
	30	6.69	26.58	0.75	4.75	39.94	72.61
	40	6.75	24.79	0.704	5.12	46.15	74.51
Fast BilateralV2	10	6.39	15.32	0.53	5.12	14.47	27.20
	20	6.73	14.93	0.28	13.20	41.91	52.16
	30	6.82	14.33	0.17	21.76	46.74	65.09
	40	6.82	13.63	0.13	33.86	47.49	71.07
Robust Bilateral	10	6.67	31.88	0.89	8.66	37.56	27.55
	20	6.77	27.54	0.76	13.30	43.44	41.18
	30	6.76	25.40	0.73	11.80	43.45	37.16
	40	6.78	24.19	0.70	9.11	43.44	29.86
Fast Accurate Bilateral	10	6.52	15.39	0.51	4.23	15.36	25.34
	20	6.66	15.32	0.40	11.41	16.82	38.17
	30	6.79	15.10	0.28	14.98	34.10	48.39
	40	6.89	14.68	0.19	19.04	42.81	60.90
OD-CNN	10	6.12	34.72	0.88	5.67	49.74	57.01
	20	6.01	31.10	0.86	5.59	49.53	59.32
	30	6.14	29.38	0.81	5.74	46.98	56.77
	40	6.13	27.18	0.78	5.97	47.52	58.78
BF-CNN	10	5.850	24.161	0.83	6.40	58.96	63.42
	20	6.154	26.724	0.78	6.61	50.94	63.62
	30	5.192	23.638	0.73	6.77	63.69	66.29
	40	5.452	17.397	0.76	7.06	63.45	74.90
ACPT	10	6.33	36.58	0.96	6.04	42.39	56.64
	20	6.43	32.58	0.91	5.03	38.92	52.01
	30	6.54	30.31	0.86	4.58	34.72	49.23
	40	6.66	28.56	0.81	5.57	38.75	53.40
Proposed	10	6.47	36.54	0.95	5.76	39.77	49.45
	20	6.56	32.58	0.90	4.71	33.09	50.29
	30	6.64	30.27	0.86	4.55	39.42	48.41
	40	6.77	28.68	0.81	4.81	41.89	57.03

Table 5 shows that at σ = 10, Rolling Guidance achieves a PSNR of approximately 5 dB, and at high noise levels the gains are insignificant. In contrast, SSIM remains below 0.1, indicating low structural fidelity in MRI images. Bitonic, Gaussian, and median filters achieve slightly higher SSIM at low noise levels but lower PSNR (by 5-6 dB), suggesting they do not reduce noise sufficiently for use with MRI data. The GBFMT and NLFMT methods exhibit strong noise-reduction properties, achieving PSNR values above 29 dB at σ = 10. Their SSIM values, however, remain very low (0.07-0.08), indicating that noise is effectively reduced, yet important anatomical structures in MRI images are not well preserved. Moreover, increasing noise variance yields a monotonically decreasing response in both methods, indicating reduced stability of the noise intensity. Although the Fast Accurate Bilateral Filter and the Fast Bilateral Filter V2 offer certain advantages over spatial filters, their performance degrades substantially as noise increases. Fast Bilateral Filter V2 achieves a good SSIM at σ = 10, but at larger noise levels, SSIM decreases, and NIQE, BRISQUE, and PIQE scores rapidly increase. It implies reduced sensitivity to high noise levels in MRI images and reduced perceived quality. The Robust Bilateral Filter is always good at all levels of noise, with PSNR (31.89 dB) and SSIM (0.895) at σ =10 and SSIM (above 0.70), respectively. The stability of optimally weighted bilateral filtering in MRI denoising is evidenced by the maintenance of perceptual and structural quality, as reflected by relatively stable NIQE and PIQE scores. The SDPM approach provides balanced performance, with consistently high SSIM values (0.74-0.81) and competitive PSNR across all noise levels. eBM3D shows good denoising performance at low noise levels, reaching a PSNR of 33.26 dB and SSIM of 0.87 at 10. The higher noise, however, reduces performance, as indicated by a PSNR of 24.79 dB and SSIM of 0.704 at σ = 40. The measures of perceptual quality indicate that there are no changes in BRISQe values, but the increasing NIQE and PIQE scores reflect poorer quality of perceiving and higher levels of artifacts. Although eBM3D is effective in noise reduction and preservation of structural integrity at even lower levels of noise, its limitations become apparent when noise levels become even higher and structural integrity is threatened, which highlights the difficulties of the conventional non-learning-based methods at higher levels of noise. OD-CNN shows strong and consistent performance across all noise levels (σ = 10–40), with PSNR values ranging from 34.72 dB to 27.18 dB and SSIM values ranging from 0.88 to 0.78. It does a good job of preserving structure and reducing noise. The perceptual quality measures (BRISQUE, NIQE, and PIQE) indicate that visual quality is acceptable, as they are fairly stable. In contrast, BF-CNN's performance is less stable. Its PSNR values are a little lower and less stable, ranging from 24.16 dB to 17.39 dB. They get worse as the noise level increases, but they still achieve good SSIM values (0.83–0.76). Also, higher BRISQUE and PIQE scores indicate that perceptual quality is deteriorating, especially in the presence of excessive noise. The fact that it has higher BRISQUE and PIQE scores, however, indicates that there is a possibility of perceptual distortions, particularly when the noise level is higher. ACPT achieves the best PSNR (36.58 dB) and SSIM (0.960) at σ = 10, which is why ACPT outperforms all other techniques investigated, and its denoising and structure-preservation effects are evident as the noise level increases. The proposed ACPT-based solution achieves the same PSNR across noise levels and slightly better perceptual quality, as indicated by lower NIQE and BRISQ scores.

7. STATISTICAL SIGNIFICANCE ANALYSIS

7.1. Two-Way ANOVA Analysis of PSNR Performance

Two-Way Analysis of Variance (ANOVA) without replication was used to confirm differences in performance across various denoising techniques statistically. The dependent variable was PSNR, and the two variables considered were the denoising technique and the noise level (σ = 10, 20, 30, and 40).

The analysis for dataset 1 revealed a statistically significant main effect of the denoising method on PSNR $F(11,33)=37.76$, $p<0.001$ indicating substantial performance variation among the evaluated algorithms. Additionally, the effect of noise level was found to be statistically significant $F(3,33)=11.91$, $p<0.001$ confirming that reconstruction quality degrades as noise intensity increases.

The analysis for dataset 2 revealed a statistically significant main effect of the denoising method $F(11,33)=50.01$, $p<0.001$ indicating substantial performance differences among the evaluated algorithms. The effect of noise level was also found to be statistically significant $F(3,33)=3.86$, $p<0.005$ confirming that increasing noise degrades reconstruction quality.

The *post hoc* multiple-comparison study employed Tukey's Honestly Significant Difference (HSD) test to further identify which specific approaches were significantly different. The results indicate that the proposed approach is statistically significantly better than a set of baseline filtering schemes (including Gaussian, median, and bilateral filters) with $p<0.05$.

Nevertheless, at lower noise levels, the differences in PSNR do not differ significantly when compared with those of the ACPT approach, which is consistent with the reported marginal numerical differences. The suggested approach yields more consistent benefits at higher noise levels, particularly for structural and perceptual quality criteria (*e.g.*, SSIM).

The results confirm that, across different noise levels, the proposed methodology leads to statistically superior denoising performance as compared to existing methods.

Table 6 shows the runtime of different denoising methods on Dataset 1 at noise levels (σ = 10–40). It is clear that basic filtering methods like Gaussian and median filters are very inexpensive to use because they operate only on small regions. Bilateral variations and Rolling Guidance are two examples of edge-preserving

filters that run quickly. More advanced non-local methods, such as NLFMT, are much more expensive to run because they require extensive patch matching and aggregation operations. Deep learning-based methods (OD-CNN and BF-CNN) are still faster than patch-based methods, but they are expensive. This is because convolutional operations add extra work. The ACPT method has the highest computational cost among the methods we examined, because it uses PCA-based processing and adaptive clustering. The suggested method incurs higher processing costs because it combines ACPT with wavelet-based refinement and co-occurrence filtering. At certain noise levels, it shows execution times similar to or shorter than ACPT, suggesting that adding extra processing steps works well. The better denoising performance and better preservation of the structure of the suggested method offset the higher cost of simple filters. The method is also primarily intended to improve medical images stored on a computer, where accuracy and perceptual quality are more important than real-time processing.

8. ABLATION STUDY

Table 7 shows the performance of the ablation study for the proposed method. At low noise levels (σ = 10), the standalone ACPT module has a high denoising ability as evidenced by a PSNR of 31.6063 dB and SSIM of 0.8912, suggesting effective noise removal. The PSNR remains almost unchanged in the case of the Co-occurrence Filter (ACPT + CoF), but the SSIM rises to 0.89153, suggesting better structure preservation as the filter can emphasise spatially correlated patterns. Likewise, the ACPT + Wavelet structure fine-tunes the high-frequency elements by offering a marginal improvement, keeping the similar PSNR and marginally improving the SSIM (0.89147). The Final Output, which combines the CoF with wavelet-based residual processing, achieves the best performance with the highest PSNR (31.6238 dB) and SSIM (0.8967), showing a better trade-off between noise suppression and structure preservation. The effectiveness of ACPT alone is more evident at relatively low noise levels (σ = 20), with PSNR and SSIM decreased to 28.0313 dB and 0.77921, respectively. The wavelet-based approach additionally stabilises the data, while the incorporation of the CoF increases the SSIM to 0.78189.9. Again, the Final Output achieves the best results (PSNR: 28.0750 dB, SSIM: 0.7913), as both components complement each other. All methods are negatively affected by the increased complexity of the noise at a higher noise level (σ = 30 and 40). But the Final Output consistently surpasses the individual components, achieving the best PSNR and SSIM values (26.2338 dB / 0.7158 at σ = 30 and 24.9805 dB / 0.6533 at σ = 40). This ablation study demonstrates that the wavelet-based residual processing enhances fine structures, the Co-occurrence Filter preserves structural integrity, and ACPTto provides a reliable baseline for noise suppression. The combination in the proposed framework is the most stable and consistent throughout all noise levels, validating the hybrid solution.

Table 6. Run time analysis for dataset 1.

Method	σ=10	σ=20	σ=30	σ=40
Rolling Guidance	1.4423	0.9317	0.7639	1.0804
Bitonic (X)	0.85	0.82	0.80	0.88
Gaussian (Y)	0.02	0.02	0.02	0.02
Median (Z)	0.05	0.05	0.05	0.05
GBFMT	3.0849	2.6343	2.1857	2.4382
NLFMT	29.5066	30.7029	28.0384	28.8969
SDPM	8.21	7.95	7.62	7.88
Fast Bilateral V2	5.8398	1.1181	1.1657	1.0436
Robust Bilateral	1.0465	1.0007	0.8941	1.3662
Fast Accurate Bilateral	1.3503	0.3973	0.5211	0.6055
OD-CNN	12.45	12.10	11.85	11.60
BF-CNN	10.32	10.05	9.88	9.60
ACPT	55.3974	33.8668	45.2401	30.5642
Proposed Method	**43.6675**	**35.2128**	**47.4554**	**36.8162**

Table 7. Performance comparison of ACPT, co-occurrence filtering, and final output at different noise levels.

Noise Level	ACPT		ACPT+Co-Occurrence		ACPT + Wavelet		Final Output	
	PSNR	SSIM	PSNR	SSIM	PSNR	SSIM	PSNR	SSIM
10	31.6063	0.8912	31.6062	0.89153	31.6045	0.89147	31.6238	0.896746
20	28.0313	0.77921	28.043	0.78189	28.0457	0.781	28.0750	0.791323
30	26.2067	0.70196	26.2055	0.70609	26.1984	0.7035	26.2338	0.715809
40	24.9368	0.63871	24.930	0.63873	24.9373	0.63997	24.9805	0.653283

Even though the PSNR difference between the proposed method and the standalone ACPT method is numerically small at lower noise levels, such subtle benefits are typical and significant in image denoising applications. More importantly, the proposed method continues to improve perceptual quality metrics (NIQE, BRISQUE, PIQE) and structural similarity (SSIM), indicating better preservation of fine details and reduced artifacts. The successive processing stages enable targeted refinement of structures that are not fully represented by ACPT and that operate in the residual domain. This results in a fairer trade-off between noise suppression and detail preservation, particularly at higher noise levels.

In the proposed architecture, the Co-occurrence Filter (CoF) is effective because it can exploit statistical spatial relationships in the residual domain. Spatial uncorrelation of the Gaussian noise means that pixel intensities vary randomly. On the other hand, fine textures and structures are highly correlated, with a consistent relationship between the intensities of proximity to nearby pixels.

The CoF analyses the co-occurrence statistics of pixel intensities within neighbourhoods in the residual (method-noise) image, which contains noise and attenuated structures. This helps to preserve structure, leading to better SSIM scores, as the ablation study demonstrated.

Examples of deep learning-based methods that have recently seen a surge in medical image denoising include convolutional neural networks, attention-based systems, and hybrid optimization systems. These methods are rather effective for modeling non-linear noise distributions and for learning complex feature representations. But the existence of large annotated datasets, time-consuming training procedures, and considerable computing resources often dictate their performance.

The proposed solution, in turn, is based on a hybrid model that is not a learning-based approach and requires no training data or parameter learning. This makes it particularly suitable for cases where computational performance is essential or annotated medical datasets are limited. The proposed approach explicitly predicts image structures *via* adaptive clustering, statistical co-occurrence analysis, and multi-scale wavelet operations, whereas deep learning methods aim to generate hierarchical feature representations.

The proposed architecture, offering a lightweight and understandable solution that maintains the same performance at various levels of noise, can be regarded as a complementary alternative to data-driven solutions, but not a direct competitor. The approaches remain applicable in actual medical imaging practice where processing overhead, consistency, and robustness are vital.

While evaluating denoising performance, it is equally important to consider data complexity and privacy, as these factors significantly impact the practicality of medical image analysis frameworks.

Recent studies have highlighted the importance of data complexity [32] and privacy [33] in the analysis of medical images. For instance, evaluations of brain MRI images predicated on data complexity indicate that the efficacy and generalizability of learning-based models are significantly influenced by fluctuations in image characteristics, including structural heterogeneity and noise distribution. This shows how difficult it is to teach data-driven methods for handling complex medical datasets. Privacy-preserving frameworks, such as decentralized recommendation systems, also demonstrate a growing need for secure data processing without centralized data sharing. It is very important to protect patient privacy and adhere to data protection standards in medical imaging, as the patient data is highly sensitive.

In this case, the suggested denoising framework offers several advantages. It reduces the risk of privacy issues because it does not rely on learning-based methods that require large training datasets or centralized data aggregation. Also, the approach is less sensitive to changes in data complexity than data-driven models, as it operates directly on individual images. The proposed framework provides a supplementary alternative that is inherently more robust to data dependence and aligns effectively with privacy-preserving standards in medical imaging applications. In contrast, deep learning methodologies are highly dependent on data availability and raise privacy concerns.

CONCLUSION

This article compares traditional spatial filters, bilateral filtering variants, non-local methods, and adaptive hybrid methods comprehensively. The experimental study of different noise levels clearly shows that most existing methods perform well only in low-noise conditions. As the noise levels increase, performance metrics such as PSNR and SSIM exhibit a linear decrease. This degradation is also evident in the deteriorated visual quality, suggesting that traditional methods are not highly sustainable in high-noise environments.

However, at both low and high noise levels, the proposed denoising algorithm consistently outperforms. Unlike current methods, the proposed method is efficient at minimizing noise, preserving both perceptual and structural information even at higher noise levels. The reported quantitative metrics are well correlated with the visual assessment results, in which increases in PSNR and SSIM are accompanied by enhanced visualization of anatomical structures. This shows that the selected performance measurements accurately reflect the quality of perceptual images. In general, the results demonstrate the effectiveness and reliability of the proposed method for practical denoising tasks, particularly in medical imaging scenarios where noise levels may vary significantly. Future work will focus on further enhancing the method for deployment in clinical and large-scale imaging systems.

To evaluate image denoising methods, this paper focuses on denoising additive Gaussian noise, a popular and controllable model. Actual medical imaging noise, such as Rician noise in MRIs or Poisson-distributed noise

in CT scans, is far more complex. The existing system does not explicitly model these noise distributions, which are primarily designed to support Gaussian noise (sensor noise). Therefore, although the proposed method may be successful with Gaussian noise, further studies are required to determine whether it can be extended to real-world clinical noise. The framework will be further developed to incorporate more realistic noise models, and its performance will be evaluated based on clinically acquired data. The present study focuses on Gaussian noise; however, real-world medical imaging applications involve larger datasets and more intricate noise characteristics. Future research will consider extending the assessment to realistic noise models and standard benchmarks.

AUTHORS' CONTRIBUTIONS

The authors confirm contribution to the paper as follows: S.A.: Data collection, implementation of methods, analysis, and writing; A.D.: Supervision, validation, review, and editing.

LIST OF ABBREVIATIONS

HRCT	=	High-Resolution Computed Tomography
MRI	=	Magnetic Resonance Imaging
PSNR	=	Peak Signal-to-Noise Ratio
SSIM	=	Structural Similarity Index Measure
NIQE	=	Natural Image Quality Evaluator
BRISQUE	=	Blind/Referenceless Image Spatial Quality Evaluator
PIQE	=	Perception-based Image Quality Evaluator
FSIM	=	Feature Similarity Index
ACPT	=	Adaptive Clustering and Progressive PCA Thresholding
PCA	=	Progressive Principal Component Analysis
CoF	=	Co-occurrence Filter
AWF	=	Adaptive Weight Function
BM3D	=	Block-Matching and 3Dimensional
HCPSO	=	Hybrid of Cuckoo Particle Swarm Optimisation
GDBF	=	Guided Decimation Box Filter
NLM	=	Non-Local Means
AMF	=	Adaptive Median Filter
MDBMF	=	Modified Decision-Based Median Filter
SURE	=	Stein Unbiased Risk Estimator
ODCNN	=	Optimal Deep Convolution Neural Network
FATL	=	Feedback Artificial Lion

ETHICS APPROVAL AND CONSENT TO PARTICIPATE

This research did not involve human participants, animal subjects, or any material that requires ethical approval.

HUMAN AND ANIMAL RIGHTS

Not applicable.

CONSENT FOR PUBLICATION

Not applicable.

DATASET AVAILABILITY

The dataset is available at repository https://github.com/Imagingscience with reference [31] in the manuscript. The following dataset link is mentioned: https://github.com/Imagingscience/Image-Fusion-Image-Denoising-Image-Enhancement-/commits?author=Imagingscience.

FUNDING

None.

CONFLICT OF INTEREST

The authors declare no conflict of interest, financial or otherwise.

ACKNOWLEDGEMENTS

Declared none.

REFERENCES

[1] Mao J, Sun L, Chen J, Yu S. Overview of research on digital image denoising methods. Sensors 2025; 25(8): 2615. http://dx.doi.org/10.3390/s25082615 PMID: 40285303

[2] Singh P. Understanding medical image denoising, enhancement, and reconstruction. Biomed Inform Smart Healthcare 2025; 1(1): 35-9. http://dx.doi.org/10.62762/BISH.2025.966762

[3] Kaur A, Dong G. A complete review on image denoising techniques for medical images. Neural Process Lett 2023; 55(6): 7807-50. http://dx.doi.org/10.1007/s11063-023-11286-1

[4] Abuya TK, Rimiru RM, Okeyo GO. An image denoising technique using wavelet-anisotropic gaussian filter-based denoising convolutional neural network for CT images. Appl Sci 2023; 13(21): 12069. http://dx.doi.org/10.3390/app132112069

[5] Sahu S, Anand A, Singh AK, Agrawal AK, Singh MP. MRI denoising using improved unbiased NLM filter. J Ambient Intell Humaniz Comput 2023; 14(8): 10077-88. http://dx.doi.org/10.1007/s12652-021-03681-0

[6] Izadi S, Sutton D, Hamarneh G. Image denoising in the deep learning era. Artif Intell Rev 2023; 56(7): 5929-74. http://dx.doi.org/10.1007/s10462-022-10305-2

[7] Jebur RS, Zabil MHBM, Hammood DA, Cheng LK, Al-Naji A. Image denoising using hybrid deep learning approach and self-improved Orca predation Algorithm. Technologies 2023; 11(4): 111. http://dx.doi.org/10.3390/technologies11040111

[8] Jebur RS, Zabil MHBM, Hammood DA, Cheng LK. A comprehensive review of image denoising in deep learning. Multimed Tools Appl 2024; 83(20): 58181-99.

[9] Darvishi Ghaleh O, Maihami V, Khamforoosh K. Medical image denoising: Techniques, challenges, and future directions. Passer J

Basic Appl Sci 2025; 7(2): 902-20.
[10] Zubair M, Md Rais HB, Ullah F, Al-Tashi Q, Faheem M, Ahmad Khan A. Enabling predication of the deep learning algorithms for low-dose CT scan image denoising models: A systematic literature review. IEEE Access 2024; 12: 79025-50. http://dx.doi.org/10.1109/ACCESS.2024.3407774
[11] Yahya AA, Tan J, Su B, *et al*. BM3D image denoising algorithm based on an adaptive filtering. Multimedia Tools Appl 2020; 79(27-28): 20391-427. http://dx.doi.org/10.1007/s11042-020-08815-8
[12] Jia H, Yin Q, Lu M. Blind-noise image denoising with block-matching domain transformation filtering and improved guided filtering. Sci Rep 2022; 12(1): 16195. http://dx.doi.org/10.1038/s41598-022-20578-w PMID: 36171466
[13] Treece G. Real image denoising with a locally-adaptive bitonic filter. IEEE Trans Image Process 2022; 31: 3151-65. http://dx.doi.org/10.1109/TIP.2022.3164532 PMID: 35394907
[14] Gautam D, Khare K, Shrivastava BP. A novel guided box filter based on hybrid optimization for medical image denoising. Appl Sci 2023; 13(12): 7032. http://dx.doi.org/10.3390/app13127032
[15] Taassori M, Vizvári B. Enhancing medical image denoising: A hybrid approach incorporating adaptive Kalman filter and non-local means with Latin square optimization. Electronics 2024; 13(13): 2640. http://dx.doi.org/10.3390/electronics13132640
[16] Kshem W, Khmag A. Improving Block Matching and 3 Dimensions (BM3D) Filtering for Image Noise Removal Using Discrete Wavelet Transformation (DWT). 2024 IEEE 4th International Maghreb Meeting of the Conference on Sciences and Techniques of Automatic Control and Computer Engineering (MI-STA). Tripoli, Libya, 2024, pp. 375-380 http://dx.doi.org/10.1109/MI-STA61267.2024.10599673
[17] Han TT, Nguyen Van H, Nguyen Huu P. Denoising Method for MRI Images Using Modified BM3D Filter with Complex Network and Artificial Neural Networks. J Electr Comput Eng 2024; 2024: 1-9. http://dx.doi.org/10.1155/2024/2606485
[18] Zangana HM, Mustafa FM. Hybrid image denoising using wavelet transform and deep learning. EAI Endorsed Transact AI Robotics 2024; 3(1): 1-32. http://dx.doi.org/10.4108/airo.7486
[19] Ullah F, Kumar K, Rahim T, Khan J, Jung Y. A new hybrid image denoising algorithm using adaptive and modified decision-based filters for enhanced image quality. Sci Rep 2025; 15(1): 8971. http://dx.doi.org/10.1038/s41598-025-92283-3 PMID: 40089479
[20] Zhang X. Improved non-local means using structural similarity for image denoising. Circuits Syst Signal Process 2025; 44(4): 2706-36. http://dx.doi.org/10.1007/s00034-024-02931-8
[21] Zhang Q, Shen X, Xu L, Jia J. Rolling Guidance Filter. In: Fleet D, Pajdla T, Schiele B, Tuytelaars T, Eds. Computer Vision – ECCV 2014. Cham: Springer 2014; pp. 815-30. http://dx.doi.org/10.1007/978-3-319-10578-9_53
[22] Ghosh S, Chaudhury KN. On fast bilateral filtering using Fourier kernels. IEEE Signal Process Lett 2016; 23(5): 570-3. http://dx.doi.org/10.1109/LSP.2016.2539982
[23] Shreyamsha Kumar BK. Image denoising based on gaussian/bilateral filter and its method noise thresholding. Signal Image Video Process 2013; 7(6): 1159-72. http://dx.doi.org/10.1007/s11760-012-0372-7
[24] Shreyamsha Kumar BK. Image denoising based on non-local means filter and its method noise thresholding. Signal Image Video Process 2013; 7(6): 1211-27. http://dx.doi.org/10.1007/s11760-012-0389-y
[25] Chaudhury KN, Dabhade SD. Fast and provably accurate bilateral filtering. IEEE Trans Image Process 2016; 25(6): 2519-28. http://dx.doi.org/10.1109/TIP.2016.2548363 PMID: 27093722
[26] Chaudhury KN, Rithwik K. Image denoising using optimally weighted bilateral filters: A sure and fast approach. 2015 IEEE International Conference on Image Processing (ICIP). Quebec City, QC, Canada, 2015, pp. 108-112. http://dx.doi.org/10.1109/ICIP.2015.7350769
[27] Shen C, Yang Z, Zhang Y. PET image denoising with score-based diffusion probabilistic models. International conference on medical image computing and computer-assisted intervention. Vancouver, BC, Canada, October 8–12. http://dx.doi.org/10.1007/978-3-031-43907-0_26
[28] Atal DK. Optimal deep CNN–based vectorial variation filter for medical image denoising. J Digit Imaging 2023; 36(3): 1216-36. http://dx.doi.org/10.1007/s10278-022-00768-8 PMID: 36650303
[29] Elhoseny M, Shankar K. Optimal bilateral filter and Convolutional Neural Network based denoising method of medical image measurements. Measurement 2019; 143: 125-35. http://dx.doi.org/10.1016/j.measurement.2019.04.072
[30] Zhao W, Lv Y, Liu Q, Qin B. Detail-preserving image denoising *via* adaptive clustering and progressive PCA thresholding. IEEE Access 2018; 6: 6303-15. http://dx.doi.org/10.1109/ACCESS.2017.2780985
[31] 2026. Dataset Available from: https://github.com/Imagingscience/Image-Fusion-Image-Denoising-Image-Enhancement-/commits?author=Imagingscience
[32] Khan AN, Bilal M, Khan SU, Khan S, Sharif M. Innovative MRI denoising using federated and transfer learning. Int J Imaging Syst Technol 2025; 35(3): e70106. http://dx.doi.org/10.1002/ima.70106
[33] Rahman MW, Khan MR, Nijim M. Privacy-preserving deep learning for disease diagnosis in medical imaging: A systematic review. IEEE Trans Consum Electron 2024; 14(1): 7248-69. http://dx.doi.org/10.1109/ACCESS.2025.3647561